PAPER

Role of thermal excitation in ultrafast energy transfer in chlorosomes revealed by two-dimensional electronic spectroscopy†

Sunhong Jun,[ab] Cheolhee Yang,[ab] Tae Wu Kim,[ab] Megumi Isaji,[c] Hitoshi Tamiaki,[c] Hyotcherl Ihee*[ab] and Jeongho Kim*[d]

Chlorosomes are the largest light harvesting complexes in nature and consist of many bacteriochlorophyll pigments forming self-assembled J-aggregates. In this work, we use two-dimensional electronic spectroscopy (2D-ES) to investigate ultrafast dynamics of excitation energy transfer (EET) in chlorosomes and their temperature dependence. From time evolution of the measured 2D electronic spectra of chlorosomes, we directly map out the distribution of the EET rate among the manifold of exciton states in a 2D energy space. In particular, it is found that the EET rate varies gradually depending on the energies of energy-donor and energy-acceptor states. In addition, from comparative 2D-ES measurements at 77 K and room temperature, we show that the EET rate exhibits subtle dependence on both the exciton energy and temperature, demonstrating the effect of thermal excitation on the EET rate. This observation suggests that active thermal excitation at room temperature prevents the excitation trapping at low-energy states and thus promotes efficient exciton diffusion in chlorosomes at ambient temperature.

Introduction

Excitation energy transfer (EET) in photosynthetic light harvesting complexes (LHCs) is a key process of photosynthesis and thus has attracted much interest with implications for solar energy applications. In photosynthetic LHCs, electronic excitations are generated by the absorption of sunlight and then transported towards the reaction centre, where charge separation occurs to generate biological energy.[1,2] For efficient funnelling of the excitation energy into the reaction centre, there should be a fine balance between energy transfer and excitation trapping, which is influenced by multiple processes, such as downhill energy migration, uphill energy transfer by thermal excitation, and phonon-assisted energy hopping.[3] In fact, the unidirectional

EET processes through many pigments in the photosystem exhibit a remarkably high efficiency close to unity. For the development of novel, high-performance optoelectronic devices, it will be desirable to understand the mechanism of such a highly efficient EET in natural photosynthesis and to ultimately learn the molecular design principles of artificial photosynthesis.[3]

Chlorosomes, the largest light harvesting complexes found in nature, are a unique family of LHCs that are composed of only bacteriochlorophyll (BChl) pigments without the support of any protein matrix. Specifically, in chlorosomes, up to hundreds of thousands of BChls are non-covalently bound to each other in a head-to-tail direction to form self-assembled aggregates *via* strong J-type excitonic coupling, resulting in a manifold of closely spaced exciton states.[4,5] The chlorosomal J-aggregates not only exhibit high exciton mobility superior to any other organic molecular systems,[6] but are also synthesizable and chemically modifiable *in vitro*.[7] Therefore, chlorosomes are envisioned as potential building blocks for nanoscale optoelectronic devices such as solar cells,[8,9] photodetectors,[10] and other excitonic devices.[11,12]

In chlorosomes, a series of EET processes occur over a broad range of time scales from tens of femtoseconds (fs) to hundreds of picoseconds (ps), while the interpretation of individual EET steps is still controversial due to (1) variation of their time scales depending on the probing technique or the type of BChls constituting chlorosomes and (2) the complex hierarchical structure of chlorosomes consisting of multi-layered tubes and/or curved lamellar layers with significant structural disorder.[13–21]

a Department of Chemistry, KAIST, Daejeon 305-701, Republic of Korea.
  E-mail: hyotcherl.ihee@kaist.ac.kr
b Center for Nanomaterials and Chemical Reactions, Institute for Basic Sciences (IBS), Daejeon 305-701, Republic of Korea
c Graduate School of Life Sciences, Ritsumeikan University, Kusatsu, Shiga 525-8577, Japan
d Department of Chemistry, Inha University, Incheon 402-751, Republic of Korea.
  E-mail: jkim5@inha.ac.kr

For example, kinetic components on the time scale of a few to tens of ps were assigned to inter-layer or inter-chlorosome EET[16,17,19–21] while the kinetics occurring in tens to hundreds of picoseconds were assigned to EET from chlorosomes to the baseplate.[14,17,19] Recently, the earliest stage of EET processes in chlorosomes was probed on the sub-100 fs time scale using two-dimensional electronic spectroscopy (2D-ES) and was assigned to downhill energy relaxation (and exciton diffusion in space) within or among coherent domains in a single layer of BChls.[22,23] In addition, coherent oscillations of the electronic origin were observed using 2D-ES, serving as an evidence of coherent energy transfer involved in the initial stage of EET in chlorosomes.[23]

The dynamics of EET among various excited states in chlorosomes as well as other photosynthetic LHCs have been studied intensely using various time-resolved spectroscopies[4,13–15,17,18,24–27] and theoretical calculations.[5,28–32] In particular, transient absorption (TA) spectroscopy has been used as a major experimental tool for investigating the EET dynamics in LHCs so far. A series of TA spectra represent transient population changes of electronic states induced by photoexcitation. However, in a TA spectrum, various features arising from different excited electronic states are overlapped with one another along an emission energy axis and therefore the interpretation of the TA spectra is often very complicated, especially for complex molecular assemblies like chlorosomes. Alternatively, TA measurements can be implemented using narrow-band pump and probe pulses so that the EET dynamics between a specific pair of electronic states can be probed selectively. However, such approach requires many measurements with various combinations of pump and probe wavelengths to cover a broad spectral range of the absorption spectra of LHCs. In contrast, 2D-ES provides 2D spectra where the contributions of various excited states are resolved in a 2D energy space (composed of absorption and emission energy axes) rather unambiguously. Also, by making use of broadband pulses, electronic transitions to various excited states in a broad spectral range and the EET among those states can be determined by a single measurement. Because a 2D spectrum measured at a specific time delay after photoexcitation provides an instantaneous snapshot of electronic coupling and energy transfer among the manifold of excited states, the analysis of a series of 2D spectra measured at various time delays after photoexcitation can help to elucidate complex pathways of energy flow in the excited states. Recently, 2D-ES has been used to map the complex pathways of EET among the manifold of excited states in LHCs and provided an evidence of coherent energy transfer associated with highly efficient EET in natural LHCs.[33–38]

In this work, we apply 2D-ES to chlorosomes to investigate the details of temperature-dependent, ultrafast EET dynamics occurring in the excited states of chlorosomes. From time evolution of the measured 2D electronic spectra, we directly mapped out the distribution of the EET rate among the manifold of closely spaced exciton states in chlorosomes in a 2D energy space. In particular, we found that the EET rate varies gradually depending on the energies of energy-donor and energy-acceptor states. In addition, from comparative 2D-ES measurements at

77 K and room temperature (RT, 293 K), we showed that the EET rate exhibits subtle dependence on both the exciton energy and temperature, demonstrating the effect of thermal excitation on the EET rate. Therefore, the 2D distribution map of the EET rate extracted from the 2D spectra reflects the Boltzmann distribution of populations in the excited states of chlorosomes at a given temperature. Based on the subtle dependence of the EET rate on the exciton energy and temperature, we infer that active thermal excitation at RT prevents the excitation trapping at low-energy states and thus can promote efficient exciton diffusion in chlorosomes at ambient temperature, which is an evidence of how cleverly Nature has designed the EET processes in photosynthetic LHCs.

Methods

Sample preparation

Chlorosomes consisting of BChl e molecules were isolated from *Chlorobaculum limnaeum* (formerly known as *Chlorobium phaeobacteroides*) 1549.[39] We prepared a diluted sample solution of chlorosomes in a 30 : 70 (v/v) mixture of 50 mM Tris-HCl buffer and glycerol and added $Na_2S_2O_4$ as a reductant. The optical density of the sample solution was 0.3 at the absorption peak in a sandwich-type sapphire cell of 0.2 mm optical path length. For the measurement at low temperature (77 K), the sample was kept in a cryostat (JANIS VPF-100) using liquid nitrogen as a coolant. For the measurement at RT (293 K), we also placed the sample in the cryostat to maintain the same experimental conditions (for example, dispersion added to the laser pulses by the front window material of the cryostat) as those for the measurement at 77 K. To prevent the effect of exciton annihilation on the decay of the 2D-ES signal, the energy of the laser pulses used for the 2D-ES measurement was adjusted to be ~1.2 nJ per pulse. The resultant excitation intensity was 5.5×10^{11} photons cm^{-2} per pulse that satisfies the exciton annihilation-free conditions.[19]

Two-dimensional electronic spectroscopy

The 2D-ES measurement was performed using a setup based on a diffractive optic, as shown in Fig. S1 in the ESI.†[23,40,41] Briefly, the 800 nm pulses of 50 fs duration generated from a 1 kHz regenerative amplified Ti:sapphire laser (Coherent Legend Elite seeded by Vitesse) were converted to visible wavelengths by a home-built noncollinear optical parametric amplifier (NOPA). The broadband NOPA output pulses of a 720 nm centre wavelength and an 80 nm bandwidth were compressed by a prism compressor. Using a diffractive optic (DO; Holoeye DE228), the incident NOPA beam was split into four beams arranged in the BOXCARS geometry. Three beams (1–3) were used to induce the 3rd-order photon echo signal, while beam 4 was attenuated by a factor of 10^3 using a neutral density filter and used as a local oscillator (LO). The accurate time delays between pulses 1, 2 and 3 were controlled by pairs of glass wedges inserted into the beams 1–3 in an anti-parallel orientation. For the 2D-ES measurement, the photon echo signal was irradiated in the $k_s = -k_1 + k_2 + k_3$ phase-matched direction, which is one corner

of the BOXCARS geometry. The LO field (beam 4), which was collinear with the signal field, got mixed with the signal and enabled the phase-sensitive heterodyne detection using the spectral interferometry. The spectral interference fringes between the signal and the LO were recorded using a spectrograph and a CCD while scanning the time delay between pulses 1 and 2 (coherence time, τ) and the delay between pulses 2 and 3 (population time, T). The coherence time τ was varied from -125 fs to $+125$ fs by a 0.25 fs increment, and the population time T was varied from 0 to 480 fs by a 5 fs increment. We obtained the absorption frequency ω_τ by Fourier transforming the measured signal along the τ axis, while the emission frequency ω_t was directly obtained by dispersed detection using a combination of a spectrograph and a CCD, thus giving a 2D spectrum. The time resolution of the experiment was determined to be 15 fs at the sample position from the non-resonant transient grating measurement of a pure solvent (carbon tetrachloride), as shown in Fig. S2 in the ESI.† The 2D spectra were phased by comparing a separately measured transient absorption spectrum and the projection of a 2D spectrum onto the ω_t axis at each T.

Results and discussion

Two-dimensional electronic spectra of chlorosomes

The steady-state absorption spectrum of BChl e chlorosomes isolated from *Chlorobaculum limnaeum* was measured at RT, as shown in Fig. S3 in the ESI.† The absorption band peak at 13 930 cm^{-1} (718 nm) is ascribed to the Q$_y$ transition of the chlorosomes. Since the chlorosomes are J-aggregates, the Q$_y$ absorption band is red-shifted compared with that of BChl e monomers (15 290 cm^{-1}; 654 nm).[42] Also, we note that the absorption spectrum measured at 77 K is red shifted by $\sim$160 cm^{-1} compared to the one measured at RT. The spectrum of the

laser pulses (see Fig. S3 in the ESI†) used in this experiment is broad enough to cover the entire Q$_y$ absorption band and therefore all the lowest exciton states of chlorosomes can be coherently excited.

Fig. 1 shows the real (absorptive) part of the 2D spectra measured at 77 K and RT at various population times, $T = 0, 20, 40, 60, 140, 240,$ and 400 fs. The principle and the experimental details of 2D-ES are described in the ESI.† It is notable that the spectrum measured at $T = 0$ contains a positive peak elongated along the diagonal at both 77 K and RT. This positive peak corresponds to the contributions from ground-state bleaching (GSB) and stimulated emission (SE) between the ground and the excited electronic states involved in the Q$_y$ transition. It can also be seen that the positive peak is slightly tilted off the diagonal, which results from strong excitonic coupling among the manifold of electronic states.[35] Besides the positive peak, two negative peaks are observed above and below the diagonal peak, and they arise from excited state absorption (ESA) into higher-lying excited states.

In the 2D spectrum measured at $T = 0$, the positive peak has a large width (600–800 cm^{-1}) along the diagonal, which indicates the presence of significant inhomogeneous broadening responsible for the broad Q$_y$ absorption band. Such a large inhomogeneous broadening is observed even in single-molecule fluorescence and absorption spectra of individual chlorosomes, which exhibit a large distribution of peak positions and widths.[43] Considering that the single-molecule spectra of individual chlorosomes at low and ambient temperatures do not show significant narrowing compared to the ensemble spectrum, the inhomogeneous broadening must be the property of a single chlorosome. Previously, the origin of the large inhomogeneous broadening in chlorosomes was ascribed to the size variation of local coherent domains within a layer of BChls.[22] A coherent domain refers to a region where strongly coupled BChl molecules have a delocalized excitonic wave function and the size of
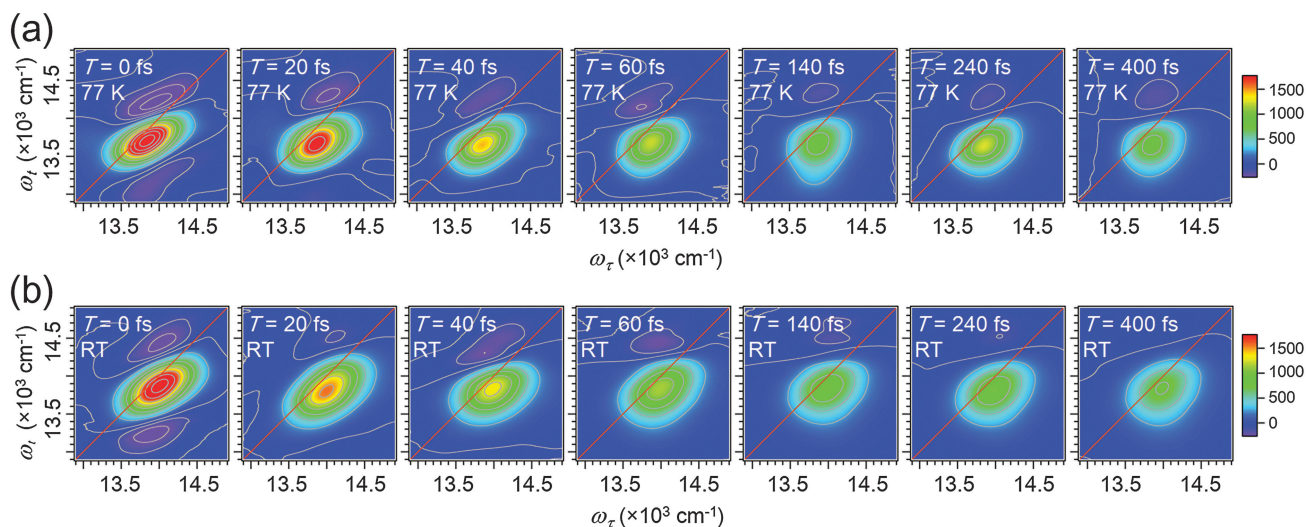

Fig. 1 2D spectra of chlorosomes at various population times at 77 K and RT. Real (absorptive) parts of 2D spectra of *Chlorobaculum limnaeum* chlorosomes measured at (a) 77 K and (b) RT. The 2D spectra at the population times of $T = 0, 20, 40, 60, 140, 240,$ and 400 fs are shown.

a coherent domain is governed by intermolecular electronic interactions and static disorder imposed by the environment.[44] In J-aggregates and organic conjugated polymers, coherent domains usually have finite sizes due to structural disorder and local defects.[45,46] While it is common that J-aggregates have narrower absorption bands than monomers due to exchange narrowing,[47] chlorosomes do not exhibit significant spectral narrowing compared to BChl *e* monomers, indicating a high level of disorder and thus significant size variation of coherent domains in chlorosomes.

Line shape dynamics of 2D spectra

As the population time (T) increases, the positive peak becomes rounder due to (1) the amplitude decrease along the diagonal and (2) the amplitude increase below the diagonal. As a result, at large T values, the round positive peak is located below the diagonal and obscures the negative ESA peak below the diagonal. The line shape change of the positive peak is completed within $T = 100$ fs and the peak shape stays almost the same thereafter. Since the change of the line shape, especially the significant amplitude increase below the diagonal, can be regarded as the growth of cross peaks below the diagonal, we can attribute the ultrafast line shape dynamics to rapid downhill energy migration towards low-energy states, as assigned in our previous work.[23] Previously, a similar downhill energy equilibration on the sub-100 fs time scale was reported for a different type of chlorosomes[22] and a photosystem I trimer from a cyanobacterium.[48]

To examine the dynamics of the line shape change quantitatively, we followed the change of diagonal and antidiagonal widths of the positive peak in the 2D spectrum. As can be seen in Fig. 2a and b, at both 77 K and RT, the diagonal width does not change much with the population time while the antidiagonal width significantly changes with the population time. Then, we defined the line shape as the ratio of the antidiagonal and the diagonal widths. The time profiles of the line shape shown in Fig. 2c were fitted using a single exponential function and we obtained the time constants of 36 fs at 77 K and 45 fs at RT, indicating that the line shape changes more slowly at RT than at 77 K. We note that the time constant for the line shape dynamics at 77 K might be underestimated because of large-amplitude coherent oscillations superimposed on the time profile. These oscillatory features arise from either vibrational or vibronic coherence created in the manifold of exciton states of chlorosomes, as discussed in detail in our previous report.[23] Also, as shown in Fig. S4 in the ESI,† we examined the dynamics of the centre line slope of the positive 2D peak as a measure of spectral relaxation dynamics[49] and found that the decay of the centre line slope at RT is slightly slower than, or comparable to, the one at 77 K. Thus, the energy relaxation toward low-energy states in chlorosomes is slightly slower at RT than at 77 K. We note that this temperature dependence of the EET rate is opposite to the trend observed for EET in other LHCs, such as the LH2 complex from purple bacteria, where the EET rate increases at higher temperature.[24]

Dependence of the EET rate on the exciton energy and temperature

To better understand the origin of this unique temperature dependence of the EET rate in chlorosomes, we examined the
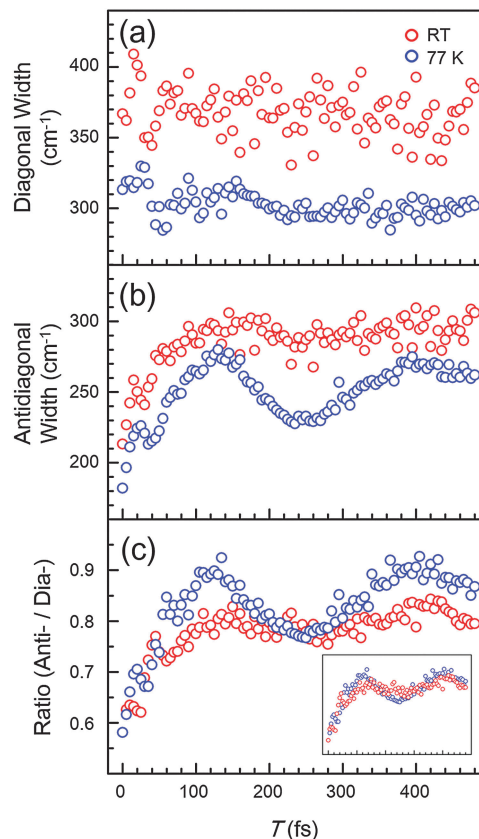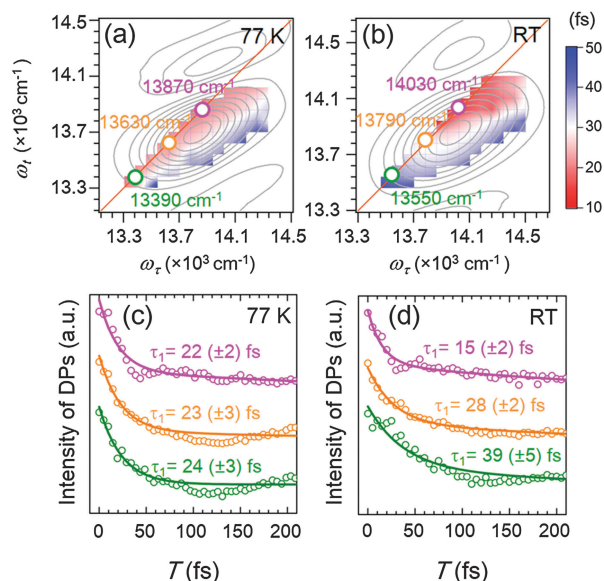

Fig. 2 (a, b) Time-dependent change of the bandwidth of a positive 2D peak in the (a) diagonal and (b) antidiagonal directions at RT (red) and 77 K (blue). The bandwidth of the peak was defined by the half-width-at-half-maximum (HWHM) of a Gaussian function that fits the slice of a 2D spectrum in the diagonal or antidiagonal direction. (c) Time evolution of the line shape defined by the ratio of antidiagonal and diagonal widths at RT (red) and 77 K (blue). The inset shows the scaled time traces of the line shape at 77 K and RT, indicating that the lines shape changes more slowly at RT than at 77 K.

decay dynamics of individual time traces at various (ω_τ, ω_t) points in the 2D spectrum. To do so, we dissected the 2D spectrum into the regions of 80 cm^{-1} × 80 cm^{-1} size and obtained a time trace of the integrated signal amplitude for each region. Then, we fitted each time trace using a sum of two exponentials and an offset and employed the time constant of a faster exponential to construct 2D distribution maps of the EET rate at two different temperatures, as shown in Fig. 3. A slower exponential and the offset were used to fit the slow decay on the time scale longer than picoseconds, which is out of the population time window (480 fs) of our experimental data. The EET rate at a specific (ω_τ, ω_t) point represents the rate at which the energy is transferred from a donor state of ω_τ energy to an acceptor state of ω_t energy. For comparison, we plotted time traces and their exponential fits at three selected diagonal points in the 2D spectra measured at 77 K and RT as shown in Fig. 3c and d, respectively. We note that the 2D distribution maps of the EET rate presented in Fig. 3a and b show only the region where the signal amplitude decays over time. In a region of lower ω_t energies further below the diagonal, we observed

This journal is © the Owner Societies 2015

Phys. Chem. Chem. Phys., 2015, **17**, 17872–17879 | 17875

Fig. 3 (a, b) The 2D distribution maps of the EET rate at (a) 77 K and (b) RT. (c, d) Individual time traces (empty dots) of the 2D-ES signal and their exponential fits (lines) at three selected diagonal points in the 2D spectrum at (c) 77 K (magenta: $\omega_\tau = \omega_t = 13\,870$ cm^{-1}, orange: $\omega_\tau = \omega_t = 13\,630$ cm^{-1}, green: $\omega_\tau = \omega_t = 13\,390$ cm^{-1}) and (d) RT (magenta: $\omega_\tau = \omega_t = 14\,030$ cm^{-1}, orange: $\omega_\tau = \omega_t = 13\,790$ cm^{-1}, green: $\omega_\tau = \omega_t = 13\,550$ cm^{-1}). Each time trace of the 2D signal was fitted using a sum of two exponentials and an offset. The time constant of a faster exponential was used for constructing the 2D distribution map shown in (a) and (b). To emphasize early-time dynamics, we show the time traces only in the population time range up to 200 fs, while the time traces in the full time range (up to 480 fs) are shown in Fig. S5 in the ESI.†

the rise of the signal amplitude in accordance with the increase of the antidiagonal width of the positive 2D peak within 100 fs. However, we were not able to resolve the rise times in that region because the rise of GSB and SE were mixed with the decay of ESA in a complicated way.

In the 2D distribution map of the EET rate, the off-diagonal EET rate below the diagonal (where $\omega_\tau > \omega_t$) represents the downhill EET rate from a donor state of ω_τ energy to an acceptor state of ω_t energy. In Fig. 3a, it can be seen that the off-diagonal EET rate decreases at both 77 K and RT as ω_t becomes smaller at a fixed ω_τ. Such change of the off-diagonal EET rate along the ω_t axis simply indicates that it takes a longer time for EET as the donor–acceptor energy separation (that is, $\omega_\tau - \omega_t$) becomes larger. The EET rate on the diagonal (where $\omega_\tau = \omega_t$) in the 2D distribution map of the EET rate reflects the net rate of population change at a specific state (caused by EET into and out of the state). In contrast to the off-diagonal rate, we can see that the diagonal EET rate changes with the exciton energy (ω_τ or ω_t) in a very different manner at RT and 77 K. Specifically, the diagonal EET rate decreases only slightly with the decrease of the exciton energy at 77 K, while it decreases considerably with the decrease of the exciton energy at RT. The subtle difference between the 2D distribution maps of the EET rate at 77 K and RT suggests that the temperature dependence of the EET rate cannot be described simply by an overall rate of the line shape change, as shown in Fig. 2. Instead, the 2D

distribution map clearly shows that the EET rate is a complex function of the temperature as well as the energies of energy-donor and energy-acceptor states.

This subtle dependence of the diagonal EET rate on both the exciton energy and temperature can be attributed to the change in the degree of thermal excitation with respect to temperature. While considering the microscopic details of EET processes, two competing factors affect the temperature dependence of the EET rate: (1) spectral overlap between an energy donor and an energy acceptor and (2) thermal excitation that controls the rate of ''uphill'' energy transfer.[50,51] Considering that the anti-diagonal width of a 2D peak reflects the degree of homogeneous broadening and is slightly larger at RT than at 77 K, the donor–acceptor spectral overlap will be larger at RT than at 77 K, predicting a faster EET at RT. In fact, we can see in Fig. 3 that the EET at exciton states of higher energies than the absorption maximum is slightly faster at RT than at 77 K. In contrast, since the thermal energy is substantially larger at RT ($kT = 206$ cm^{-1}) than at 77 K ($kT = 53$ cm^{-1}), the uphill transfer will be much more active at RT than at 77 K. As a result, the diagonal EET rate substantially decreases at low-energy states, which can be readily excited to higher-energy states by thermal energy available at RT. Accordingly, we can see in Fig. 3b that EET becomes significantly slower at the exciton states with energies lower than $\sim 13\,790$ cm^{-1}, which lie higher by $\sim kT$ (at RT) from the lowest-energy state. Thus, each of the 2D distribution maps of the EET rate shown in Fig. 3 reflect the Boltzmann distribution of populations in the excited states of chlorosomes at a given temperature.

The temperature dependence of the EET rate observed in chlorosomes seems to be different from the trend observed in other LHCs, for example, LH2 and LH3 complexes.[24,27,29] In the LH2 complex, the EET from B800 to B850 was found to be faster at RT (0.7 ps) than at 77 K (1.8 ps).[24] Also, the B800-to-B820 EET is faster at RT (0.75 ps) than at 77 K (0.9 ps) in the LH3 complex.[27,29] In these LHCs, the slower EET at 77 K was ascribed to the decreased donor–acceptor spectral overlap at low temperatures. Here we note that the energy gap between the exciton states of B800 and B850/B820 (734 cm^{-1} for B800–B850 and 306 cm^{-1} for B800–B820) is relatively large compared with the thermal energy at RT (206 cm^{-1}). As a result, the thermal excitation at RT does not directly affect the rate of EET between B800 and B850 (or B820) while it might still facilitate the EET by activating uphill transfer from dark ''trap'' states within B800. However, even for intra-B800 EET, the EET rate was observed to be faster at RT (300 fs) than at 77 K (400 fs)[24] while the same temperature dependence (80–100 fs at RT; 250–300 fs at 19 K) was observed for EET within B850.[25] Such a different temperature dependence of EET dynamics in chlorosomes and B800 (or B850) can be attributed to the difference in the electronic structure of chlorosomes and B800 (or B850). The B800 and B850 rings consist of nine and eighteen BChl a molecules, respectively,[52] while a BChl layer of chlorosomes consists of tens of thousands of BChl molecules.[53] As a result, the energy spacing between the neighbouring exciton states should be much smaller in chlorosomes than in B800 or B850,[5,28,52,54]

making the EET dynamics in chlorosomes more sensitively affected by thermal excitation. Thus, the energy and temperature dependence of the EET rate observed in chlorosomes is characteristic of the manifold of exciton states with inter-neighbour-state energy gaps smaller than thermal energy at RT.

Role of thermal excitation in excitation energy transfer

Here we can consider the implication of the unique energy and temperature dependence of the EET rate for the efficiency of EET processes in chlorosomes. At a glance, the slower EET around low-energy states observed at RT seems to be detrimental to the efficient energy flow in chlorosomes. However, when we view such a variation of the EET rate from a microscopic viewpoint, we can clearly see how cleverly Nature has designed the EET process in photosynthetic LHCs. Excitation that is initially generated at high-energy exciton states in a coherent domain is transferred to lower-energy exciton states within the same domain (that is, energy equilibration) or in the neighbouring domains (that is, exciton diffusion) until it reaches, on average, the most populated exciton states at a given temperature. Such a downhill excitation migration is independent of temperature and serves as the main driving force for exciton diffusion at low temperatures. At low temperatures, the most populated state is located in a low-energy region with a relatively low density of states (DOS) (that is, a large energy spacing between neighbouring states),[5] as schematically shown in Fig. 4 and therefore the excitation can be trapped at those states easily. As a result, the efficiency of exciton diffusion to neighbouring domains will be low. However, at RT, thermal excitation (and uphill transfer) is more active and allows the excitation to escape the trap states and climb to higher-energy states. As a result, the most populated exciton states at RT are formed in a higher-energy region with higher DOS than the ones at 77 K (see Fig. 4), thus providing more neighbouring coherent domains of similar energies into which the excitations can be transferred *via* phonon-assisted energy hopping. Thus, as schematically described in Fig. 4, thermal activation of uphill transfer at RT promotes efficient EET among coherent domains, making the ambient temperature a more favourable environment for exciton diffusion in chlorosomes.

In fact, the importance of thermal excitation in EET has been noted in other light harvesting systems. For example, photosystem I (PSI) has the so-called "red" forms of chlorophylls (Chls) that absorb at longer wavelengths than the primary electron donor, P700, of the reaction centre.[55] The low-energy states of these red Chls can trap the excitations and hinder EET to the reaction centre. As a result, thermal activation is required to achieve efficient energy flow into the reaction centre. Also, in a variant of chlorosomes (*Chlorobium tepidum*) different from the one used in this work, the effect of thermal excitation on EET was observed in a previous TA study.[16] In that work, the authors reported that a 1.7 ps kinetic component, which was assigned to a single-step inter-chlorosome EET, has smaller contributions to the amplitude decay of the TA signal at low temperatures. This observation suggests that the inter-chlorosome EET occurs from higher-energy exciton states rather than low-energy states and thus thermal population of these higher-energy states is
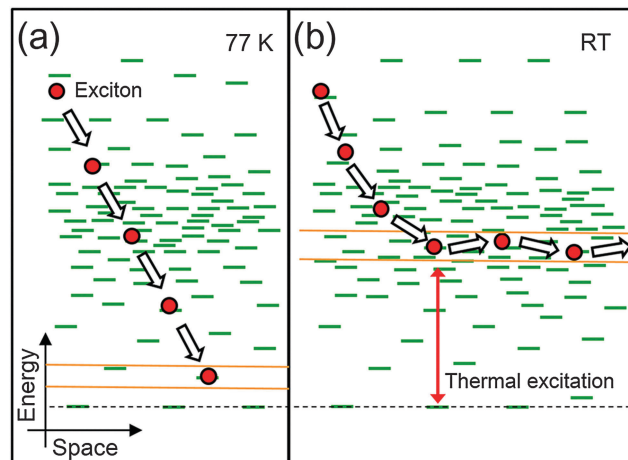

Fig. 4 Schematic illustration of downhill excitation energy transfer and exciton diffusion in chlorosomes at (a) 77 K and (b) RT. The green bars represent exciton states of chlorosomes and the red dots represent excitations populated in specific exciton states. The arrows indicate the movement of excitations in energy (vertical axis) and space (horizontal axis). A pair of orange lines denotes the most populated exciton states at a given temperature. The most populated exciton states at RT (b) have higher energies than the most populated states at 77 K (a) due to more active thermal excitation at RT. As a result, the exciton diffusion to neighbouring coherent domains is facilitated at RT *via* thermally activated energy hopping.

important for efficient EET. Besides the natural photosynthetic LHCs, the role of thermal excitation was also noted for conjugated polymers, which are artificial light harvesters. From time-resolved PL measurements on polymer–fullerene heterostructures for organic photovoltaics, it was found that the exciton diffusion length and the diffusion coefficient increase significantly at temperatures higher than 150 K.[56] The increased rate and length of spatial exciton diffusion at higher temperatures were ascribed to the increase of thermal excitation, which leads to stronger exciton–phonon coupling and more efficient energy hopping *via* phonon absorption by excitons. Considering that chlorosomes have similar structural motifs (that is, aggregates of pigments that are separated by structural disorder) as conjugated polymers to some extent, we can qualitatively infer that the spatial exciton diffusion in the natural system of chlorosomes may behave in a similar manner as in the artificial system of conjugated polymers.

Herein, we can consider the origin of the ultrafast EET dynamics presented in this work in connection with the internal organization of BChls in chlorosomes. A previous 2D-ES study on *Chlorobium tepidum* reported a 40 fs decay of the 2D signal amplitude, which is in close agreement with our result, and the origin of the fast dynamics was explained by a model of incoherent exciton diffusion among coherent domains in the same layer, especially rapid localization towards low-energy domains.[22] Meanwhile, theoretical studies on EET in chlorosomes predicted that both intra-layer EET in a single layer and layer-to-layer EET in a multi-walled tube or lamellar structure can occur as fast as 25 fs, which matches the time scale reported in our work.[5,31] Since these two processes can occur on a similar time scale and are not distinguishable from each other by

spectroscopic measurements, both types of EET processes presumably contribute to the ultrafast decay of the 2D-ES signal. For the intra-layer EET, we cannot rule out the possibility that coherent energy transfer is involved in this very first step of EET in chlorosomes, as was evidenced by the coherent oscillations (superimposed on the decay of 2D-ES signal) that arises from the coherence of the electronic origin.[23] We note that the temperature dependence of the EET rate reported in this work applies to the very early steps of EET in chlorosomes, but not necessarily to slower EET processes, for example, inter-chlorosome EET or chlorosome-to-baseplate EET. In particular, compared with BChls located in the same layer, the ones belonging to different layers or different chlorosomes will have much weaker interactions with each other, resulting in a lower probability of EET and a lower EET rate. Accordingly, the dependence of the EET rate on temperature or exciton energy can be different from the one observed for the earliest EET step found in this work.

Conclusion

We directly demonstrated the dependence of the EET rate on the exciton energy and temperature in chlorosomes by mapping out the 2D distribution of the EET rate using the powerful 2D-ES technique. This subtle dependence of the EET rate on the exciton energy and temperature provides an evidence of how Nature has designed the LHCs to be optimized for the most efficient EET at ambient temperature. The detailed EET dynamics in chlorosomes revealed in this work directly show that the EET processes occurring in the manifold of closely spaced electronic states are governed by the law of thermodynamics.

Acknowledgements

References

1 H. van Amerongen, L. Valkūnas and R. van Grondelle, *Photosynthetic Excitons*, World Scientific, 2000.

2 R. E. Blankenship, *Molecular Mechanisms of Photosynthesis*, 2nd edn, Wiley-Blackwell, 2014.

3 G. D. Scholes, G. R. Fleming, A. Olaya-Castro and R. van Grondelle, *Nat. Chem.*, 2011, **3**, 763–774.

4 N.-U. Frigaard and D. A. Bryant, in *Complex Intracellular Structures in Prokaryotes*, ed. J. M. Shively, Springer Berlin Heidelberg, 2006, vol. 2, pp. 79–114.

5 J. M. Linnanto and J. E. I. Korppi-Tommola, *J. Phys. Chem. B*, 2013, **117**, 11144–11161.

6 *J-Aggregates*, ed. T. Kobayashi, World Scientific, Singapore, 2012.

7 S. Shoji, T. Hashishin and H. Tamiaki, *Chem. – Eur. J.*, 2012, **18**, 13331–13341.

8 M. Fanshun and T. He, *Solar Cells Based on Cyanine and Polymethine Dyes*, CRC Press, 2005.

9 M. Hiramoto, K. Kitada, K. Iketaki and T. Kaji, *Appl. Phys. Lett.*, 2011, **98**, 023302.

10 G. M. Akselrod, B. J. Walker, W. A. Tisdale, M. G. Bawendi and V. Bulovic, *ACS Nano*, 2011, **6**, 467–471.

11 Y. Y. Kuznetsova, M. Remeika, A. A. High, A. T. Hammack, L. V. Butov, M. Hanson and A. C. Gossard, *Opt. Lett.*, 2010, **35**, 1587–1589.

12 G. Grosso, J. Graves, A. T. Hammack, A. A. High, L. V. Butov, M. Hanson and A. C. Gossard, *Nat. Photonics*, 2009, **3**, 577–580.

13 S. Savikhin, Y. Zhu, S. Lin, R. E. Blankenship and W. S. Struve, *J. Phys. Chem.*, 1994, **98**, 10322–10334.

14 S. Savikhin, P. I. van Noort, Y. Zhu, S. Lin, R. E. Blankenship and W. S. Struve, *Chem. Phys.*, 1995, **194**, 245–258.

15 S. Savikhin, P. I. van Noort, R. E. Blankenship and W. S. Struve, *Biophys. J.*, 1995, **69**, 1100–1104.

16 J. Pšenčík, T. Polívka, P. Němec, J. Dian, J. Kudrna, P. Malý and J. Hála, *J. Phys. Chem. A*, 1998, **102**, 4392–4398.

17 V. I. Prokhorenko, D. B. Steensgaard and A. R. Holzwarth, *Biophys. J.*, 2000, **79**, 2105–2120.

18 J. Pšenčík, Y. Z. Ma, J. B. Arellano, J. Garcia-Gil, A. R. Holzwarth and T. Gillbro, *Photosynth. Res.*, 2002, **71**, 5–18.

19 J. Pšenčík, Y.-Z. Ma, J. B. Arellano, J. Hála and T. Gillbro, *Biophys. J.*, 2003, **84**, 1161–1179.

20 J. Martiskainen, J. Linnanto, R. Kananavičius, V. Lehtovuori and J. Korppi-Tommola, *Chem. Phys. Lett.*, 2009, **477**, 216–220.

21 J. Martiskainen, J. Linnanto, V. Aumanen, P. Myllyperkiö and J. Korppi-Tommola, *Photochem. Photobiol.*, 2012, **88**, 675–683.

22 J. Dostal, T. Mancal, R. Augulis, F. Vacha, J. Pšenčík and D. Zigmantas, *J. Am. Chem. Soc.*, 2012, **134**, 11611–11617.

23 S. Jun, C. Yang, M. Isaji, H. Tamiaki, J. Kim and H. Ihee, *J. Phys. Chem. Lett.*, 2014, **5**, 1386–1392.

24 S. Hess, E. Akesson, R. J. Cogdell, T. Pullerits and V. Sundström, *Biophys. J.*, 1995, **69**, 2211–2225.

25 S. Savikhin and W. S. Struve, *Chem. Phys.*, 1996, **210**, 91–100.

26 J. Yang, M.-C. Yoon, H. Yoo, P. Kim and D. Kim, *Chem. Soc. Rev.*, 2012, **41**, 4808–4826.

27 Y.-Z. Ma, R. J. Cogdell and T. Gillbro, *J. Phys. Chem. B*, 1998, **102**, 881–887.

28 J. Strümpfer and K. Schulten, *J. Chem. Phys.*, 2009, **131**, 225101.

29 J. M. Linnanto and J. E. I. Korppi-Tommola, *Chem. Phys.*, 2009, **357**, 171–180.

30 A. W. Chin, J. Prior, R. Rosenbach, F. Caycedo-Soler, S. F. Huelga and M. B. Plenio, *Nat. Phys.*, 2013, **9**, 113–118.

31 J. Huh, S. K. Saikin, J. C. Brookes, S. Valleau, T. Fujita and A. Aspuru-Guzik, *J. Am. Chem. Soc.*, 2014, **136**, 2048–2057.

32 T. Fujita, J. Huh, S. Saikin, J. Brookes and A. Aspuru-Guzik, *Photosynth. Res.*, 2014, **120**, 273–289.

33 T. Brixner, J. Stenger, H. M. Vaswani, M. Cho, R. E. Blankenship and G. R. Fleming, *Nature*, 2005, **434**, 625–628.

34 G. S. Engel, T. R. Calhoun, E. L. Read, T. K. Ahn, T. Mancal, Y. C. Cheng, R. E. Blankenship and G. R. Fleming, *Nature*, 2007, **446**, 782–786.

35 D. Zigmantas, E. L. Read, T. Mančal, T. Brixner, A. T. Gardiner, R. J. Cogdell and G. R. Fleming, *Proc. Natl. Acad. Sci. U. S. A.*, 2006, **103**, 12672–12677.

36 E. E. Ostroumov, R. M. Mulvaney, R. J. Cogdell and G. D. Scholes, *Science*, 2013, **340**, 52–56.

37 J. M. Womick and A. M. Moran, *J. Phys. Chem. B*, 2009, **113**, 15747–15759.

38 K. L. Wells, P. H. Lambrev, Z. Zhang, G. Garab and H.-S. Tan, *Phys. Chem. Chem. Phys.*, 2014, **16**, 11640–11646.

39 H. Tamiaki, S. Tateishi, S. Nakabayashi, Y. Shibata and S. Itoh, *Chem. Phys. Lett.*, 2010, **484**, 333–337.

40 J. Kim, V. M. Huxter, C. Curutchet and G. D. Scholes, *J. Phys. Chem. A*, 2009, **113**, 12122–12133.

41 A. Nemeth, J. Sperling, J. Hauer, H. F. Kauffmann and F. Milota, *Opt. Lett.*, 2009, **34**, 3301–3303.

42 N.-U. Frigaard, K. L. Larsen and R. P. Cox, *FEMS Microbiol. Ecol.*, 1996, **20**, 69–77.

43 Y. Tian, R. Camacho, D. Thomsson, M. Reus, A. R. Holzwarth and I. G. Scheblykin, *J. Am. Chem. Soc.*, 2011, **133**, 17192–17199.

44 L. D. Bakalis and J. Knoester, *J. Phys. Chem. B*, 1999, **103**, 6620–6628.

45 P. Anderson, *Phys. Rev.*, 1958, **109**, 1492–1505.

46 H. Fidder, J. Knoester and D. A. Wiersma, *J. Chem. Phys.*, 1991, **95**, 7880–7890.

47 E. W. Knapp and S. F. Fischer, *Chem. Phys. Lett.*, 1984, **103**, 479–483.

48 J. M. Anna, E. E. Ostroumov, K. Maghlaoui, J. Barber and G. D. Scholes, *J. Phys. Chem. Lett.*, 2012, **3**, 3677–3684.

49 S. Park, K. Kwak and M. D. Fayer, *Laser Phys. Lett.*, 2007, **4**, 704–718.

50 Y. Jia, J. M. Jean, M. M. Werst, C. K. Chan and G. R. Fleming, *Biophys. J.*, 1992, **63**, 259–273.

51 M. Werst, Y. Jia, L. Mets and G. R. Fleming, *Biophys. J.*, 1992, **61**, 868–878.

52 A. M. van Oijen, M. Ketelaars, J. Köhler, T. J. Aartsma and J. Schmidt, *Science*, 1999, **285**, 400–402.

53 G. T. Oostergetel, M. Reus, A. Gomez Maqueo Chew, D. A. Bryant, E. J. Boekema and A. R. Holzwarth, *FEBS Lett.*, 2007, **581**, 5435–5439.

54 V. I. Prokhorenko, D. B. Steensgaard and A. R. Holzwarth, *Biophys. J.*, 2003, **85**, 3173–3186.

55 B. Gobets and R. van Grondelle, *Biochim. Biophys. Acta, Bioenerg.*, 2001, **1507**, 80–99.

56 O. V. Mikhnenko, F. Cordella, A. B. Sieval, J. C. Hummelen, P. W. M. Blom and M. A. Loi, *J. Phys. Chem. B*, 2008, **112**, 11601–11604.

This journal is © the Owner Societies 2015

Phys. Chem. Chem. Phys., 2015, **17**, 17872–17879 | **17879**